A Buried-Interface-Modification Strategy for Efficient Tin-Based Perovskite Light-Emitting Diodes

Zheng Jiang[1#], Jie Yang[2#], Wenbin Wang[1], Yangyu Liu[3], Yuhan Zhou[3], Jing Xu[3], Wang Wang[2], Hongyao Ding[1], Ya Zhong[1], Haifeng Zhao[4,5], Sai Bai[4], Weidong Xu[6], Wing Chung Tsoi[8], Tao Yu[3], Chunxiong Bao[3], Xiaodong Shen[1]*, Pengpeng Teng [1,7]*

[1]Jiangsu Collaborative Innovation Center for Advanced Inorganic Functional Composites, College of Materials Science and Engineering, Nanjing Tech University, Nanjing, 211816 China

[2]Key Laboratory of Flexible Electronics (KLOFE), Institute of Advanced Materials (IAM) & School of Flexible Electronics (Future Technologies), Nanjing Tech University (NanjingTech), Nanjing, China

[3]National Laboratory of Solid State Microstructures, Collaborative Innovation Center of Advanced Microstructures, School of Physics, Nanjing University, Nanjing 210093, China

[4]Institute of Fundamental and Frontier Science, University of Electronic Science and Technology of China (UESTC), Chengdu 610054, China

[5]Yibin Institute of UESTC, University of Electronic Science and Technology of China (UESTC), Yibin 644005，China

[6]Institute of Flexible Electronics (IFE), Northwestern Polytechnical University, 127 West Youyi Road, Xi'an 710072, China.

[7]Quechen Silicon Chemical Co., Ltd

[8]SPECIFIC, Faculty of Science and Engineering, Swansea University, Bay Campus, Fabian Way, Swansea SA1 8EN, United Kingdom.

[#] These authors contributed equally: Zheng Jiang and Jie Yang.

*Correspondence to Xiaodong Shen (xdshen@njtech.edu.cn); Pengpeng Teng (ppteng@njtech.edu.cn).

Abstract

Tin (Sn)-based perovskites show great potential for environmentally friendly and high-performance light-emitting diodes (LEDs). However, the development of Sn-based perovskite LEDs (PeLEDs) lags significantly behind that of lead-based perovskites. This is mainly due to the faster crystallization rate of Sn-based perovskites that leads to a higher defect density in Sn-based perovskite films, thereby serious non-radiative recombination. Here, we demonstrated a buried-interface-modification (BIM) strategy to regulate the crystallization kinetics of Sn-based perovskite films by using carboxylate as multifunctional surface modifiers. We reveal that the buried interface is critical to improve the nucleation and crystallization of Sn-based perovskite films. As a result, efficient near-infrared Sn-based PeLEDs were achieved with an external quantum efficiency (EQE) of 11.9%. This work suggests an efficient and elegant route to obtain high-performance Sn-based perovskite films and devices.

Introduction

Metal halide perovskites have emerged as promising candidates for next-generation light-emitting diodes (LEDs), which is mainly due to their low-cost solution fabrication, excellent photoluminescence, good charge mobility, high color purity, and tunable bandgap.[1-4] Despite the efficiency of perovskite LEDs (PeLEDs) having surpassed 30%,[5-7] the high-performance devices all contain toxic lead (Pb) element, which raised concerns about environment and health issues.[8, 9] Recently, tin (Sn)-based perovskites have been regarded as one of the best alternatives for their analogous optoelectronic properties.[10-13] However, the performance of Sn-based PeLEDs lags far behind their Pb counterparts. The low external quantum efficiency (EQE) of Sn-based PeLEDs is mainly due to the presence of high density of defects caused by the faster crystallization rate compared with Pb-based perovskites, which results in serious non-radiative recombination.[14-17]

Buried interface is crucial for high-quality perovskite films. It has been investigated that buried interface engineering can modulate Gibbs free energy of the perovskite precursor solution and control the crystal nucleation and growth of perovskite films, which has been proven to effectively improve the quality of Pb-based perovskite films.[18-20] However, the nucleation and crystallization control strategies developed in Pb-based PeLEDs cannot expected to be straightforwardly translated to Sn-based PeLEDs due to the remarkably difference of chemical composition.[21-23] Therefore, the effect of the buried interface to the nucleation and crystal growth mechanism of Sn-based perovskite films are still not well understood.

In this work, we demonstrate a facile buried-interface-modification (BIM) strategy to control the nucleation and growth process, which was investigated to improve quality of Sn-based perovskite films effectively. By introducing carboxylate such as formamidine acetate (FAAc) as multifunctional modifiers on the interfaces of Sn-based PeLEDs, nucleation sites of Sn-based perovskite films were increased and crystallization rate was retarded. As a result, high quality Sn-based perovskite films with a lower defect density were achieved, which leads to high-performance near-infrared (NIR) Sn-based PeLEDs with EQE of 11.9%. This value represents the most effective NIR Sn-based PeLEDs.

Results and discussion

We prepared Sn-based perovskites from precursors with the stoichiometry of FAI: CsI: SnI_2: additives= 0.9: 0.1: 1.0: x, where additives are SnF_2, PEAI and Vitamin B1.[10] The SnF_2 was used to inhibits tin oxidation and promotes uniform grain distribution, PEAI's strong hydrogen bonding with FAI enhances crystallinity, and Vitamin B1's steric hindrance effectively prevents perovskite nanocrystal aggregation (Figure S1 and S2a). We also provided the summary of average EQE values and detailed performance parameters with various additives in Figure S2b and Supplementary Table 1, respectively, from which we find that multiple additives (control) result in considerable enhancement in terms of both radiance and EQE values. The schematic process of the interface modification was shown in Figure S3. Briefly, FAAc was introduced as a modifier to treat the PEDOT:PSS substrate, rather than being directly added to the perovskite precursor or used for post-treatment — strategies that were proven to effectively improve crystal quality of perovskite films.[24-28]

We fabricated Sn-based perovskite films on different substrates to compare the effect of buried interface on crystallization. To analyze the surface characteristics of unmodified PEDOT:PSS substrate (Control) and FAAc-modified substrate (With FAAc), we measured the contact angle of perovskite precursor solution on the two substrates (**Figure 1a, b**). The contact angle of the perovskite precursor solution on PEDOT:PSS and FAAc-modified PEDOT:PSS substrate is ~20.6° and ~15.6°, respectively. The reduction of contact angle suggests the improved surface wettability of our FAAc-modified PEDOT:PSS, which can be attributed to the hydrophilic nature of carboxyl.[29] The carboxyl in FAAc has smaller size than sulphonate in PEDOT:PSS, so they can form a denser hydrogen bond network at the buried interface, thereby reducing the contact angle.[22] As shown in **Figure 1c-d**, the morphology of perovskite films before and after thermal annealing on both substrates was revealed by scanning electron microscopy (SEM). Before the annealing, the control sample (perovskite

films on PEDOT:PSS) showed poor uniformity with some crystal aggregation. In contrast, the perovskite film on FAAc-modified PEDOT:PSS showed the uniform and more nucleation sites for the growth of Sn-based perovskite films. These results are probably due to the fact that FAAc modification can reduce Gibbs free energy of the perovskite precursor solution and facilitate nucleation.[21]

According to the classical nucleation theory, the Gibbs free energy of heterogeneous nucleation (ΔG_{het}) can be expressed as equations (1) and (2):[30, 31]

$$\Delta G_{het} = \Delta G_{hom} * f(\theta) \qquad (1)$$

$$f(\theta) = \frac{1}{4}(2 - 3\cos\theta + 3cos^3\theta) \qquad (2)$$

Where ΔG_{hom} is the Gibbs free-energy of homogeneous nucleation, $f(\theta)$ is the contact angle factor, θ represents the contact angle. Besides, it is worth noting that all the perovskite films show leaf like morphological features, as the FAAc interface layer enhances nucleation sites for the growth of tin-based perovskite films, thus exhibiting more uniformity with smaller grains (**Figure 1e-f**).

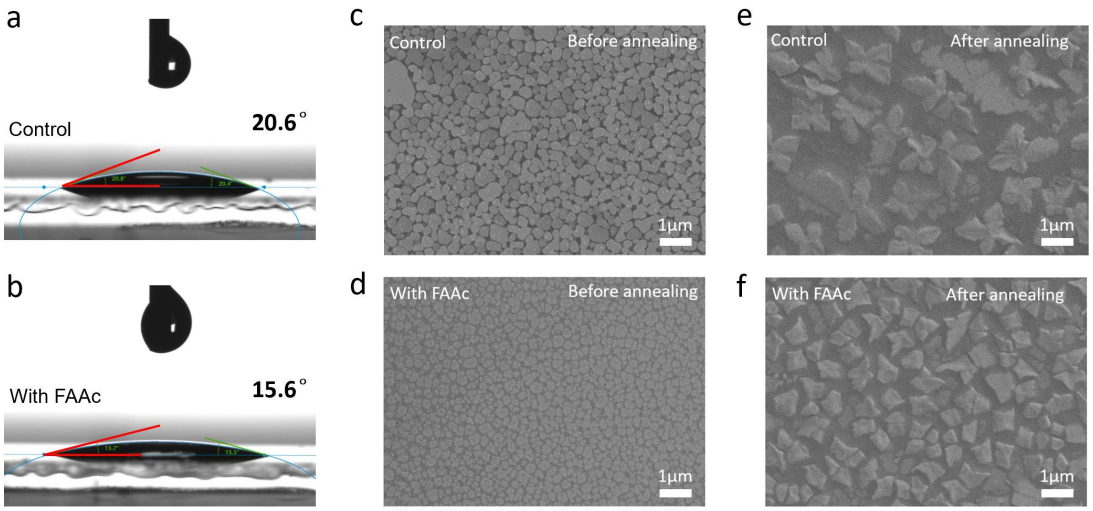

Figure 1. (a, b) The contact angle of perovskite precursor solution without (a) and with FAAc (b) on PEDOT:PSS substrate. (c-f) SEM images of $FA_{0.9}Cs_{0.1}SnI_3$ perovskite films without and with FAAc before (c, d) and after annealing (e, f), respectively.

In order to investigate the growth process of Sn-based perovskite films on the two

substrates, in-situ UV-vis and PL measurements were performed during the annealing process. Firstly, the absorption of the perovskite precursor films was studied by in-situ UV-vis spectrometry. Within the first 6 s the absorption below 900 nm continuously increases suggesting the formation of Sn-based perovskites on the PEDOT:PSS substrate. After that, the absorption became constant indicating that the reaction is complete and reflecting the fast crystallization process of Sn-based perovskite films (**Figure 2a**). For the absorption of Sn-based perovskite films on FAAc-modified substrate, the growth time was much longer (over 20 s to reach a constant) (**Figure 2b**). Then, we conducted in-situ PL measurements to provide direct proof of the evolution of crystal growth and defect formation during the perovskite crystallization process. As shown in **Figure 2c-f**, the perovskite emitters on PEDOT:PSS substrate form at around 4 s from the start of annealing process, followed by a fast rise of PL intensity and a blue-shift of PL peak, which suggests a rapid growth of crystals. The drop in PL intensity from 12 s to 24 s can be attributed to the formation of numerous defect-rich crystals. After that, the PL peak position kept constant and the PL intensity increased to a stable value. Remarkably, the PL characteristic is very different when FAAc was introduced to modify the surface of PEDOT:PSS. The PL intensity of the perovskite films prepared on the FAAc-modified substrate increased for 60 s which could be caused by much slower crystallization process. Therefore, the introduce of FAAc can suppress grain aggregation which can lead to high density of defects, therefore reduce PL quenching and non-radiative recombination.[32] Additionally, FAAc can diffuse into the perovskite layer, which was confired by O 1s XPS spectra (Figure S4), suggesting that the enhancement of PL could also result from defects passivation within the perovskite bulk. The intensity of the PL is twice that of the samples without FAAc, conforming the higher efficiency of luminescence.

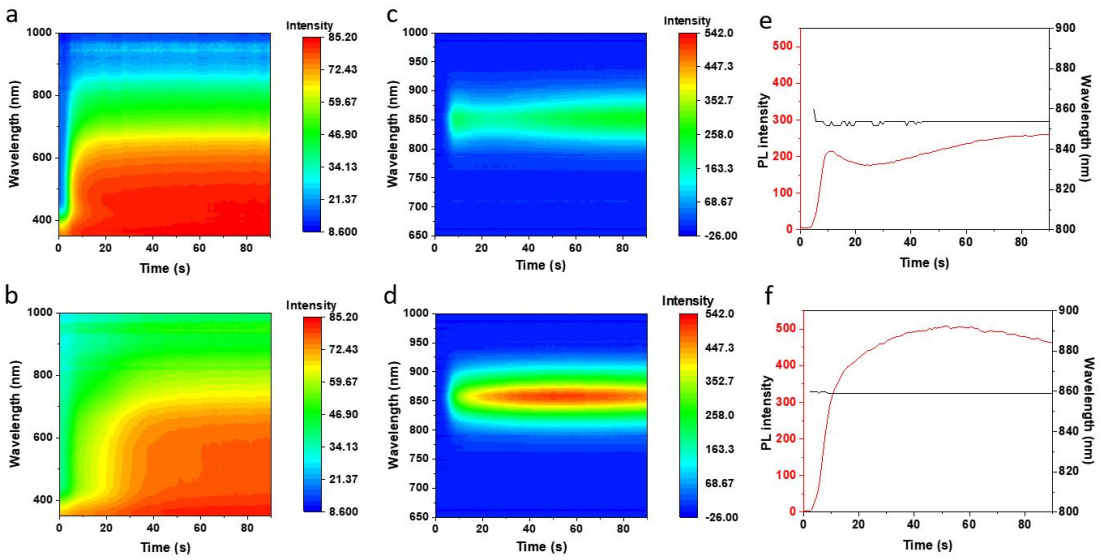

Figure 2. (a, b) In-situ UV-vis measurements of Sn-based perovskites without (a) and with FAAc (b) during the annealing process. (c-f) In-situ PL measurements of Sn-based perovskites without (c, e) and with FAAc (d, f) during the annealing process.

To further understand the properties of Sn-based perovskite films with and without FAAc modification, we proceed to investigate the crystallinity through X-ray diffraction (XRD). As illustrated in **Figure 3a**, both of the perovskite films have obvious diffraction peaks at 13.9° and 28.2° correspond to the (100) and (200) crystal planes of $FA_{0.9}Cs_{0.1}SnI_3$ perovskite. The relative intensities of (100) to (200) after FAAc modification increased from 1.16 to 1.79, suggesting enhanced preferred grain orientation. We observed that the full-width at half-maximum (FWHM) of the XRD diffraction peaks increased, indicating that the crystallite size became smaller, which likely led to the reduction in XRD diffraction intensity. The blue-shift of PL peak with FAAc at room temperature further confirms the XRD results (Figure S5). We further compare the properties of the films by assessing photoluminescence quantum yields (PLQYs) as well as PL lifetime by Time-resolved PL (TRPL) technique, and the results are shown in **Figure 3b and 3c**, respectively. Compared with the control samples, the PLQYs of perovskite films on FAAc-modified substrate enhanced dramatically. In addition, the transient PL lifetime of the films on FAAc-modified

substrate also significantly increases, suggesting lower density of defects caused by the slower crystallization process and suppressed trap-assisted non-radiative recombination. The density of defects (N_{trap}) was calculated through space charge limited current (SCLC) method (**Figure 3d**) by the equation:[33]

$$N_{trap} = \frac{2\,\varepsilon_r \varepsilon_0 V_{ETL}}{ed^2} \qquad (3)$$

Where $\mathcal{E}_r$ is relative dielectric constant of perovskite, $\mathcal{E}_0$ is vacuum dielectric constant, e is elementary charge, d is perovskite film thickness, V_{TFL} is trap-filled limit voltage. The defects density decreased from 1.33x10^{18} cm^{-3} to 1.07x10^{18}cm^{-3} after FAAc midification, which verified the above results.

Next, we investigated the role of FAAc at the interface of PEDOT:PSS/tin-based perovskite. The FAAc-modified PEDOT:PSS was washed with DMSO to simulate the actual situation of perovskite solution spin coating on the substrate. The X-ray photoelectron spectroscopy (XPS) results shown an increase of O-H on the surface of PEDOT:PSS (**Figure 3e**), since FAAc contains a higher concentration of O-H. The formation of hydrogen bonding between FAAc and PSS (Figure S6) prevents the modifier from being completely rinsed away by the perovskite solution. We further carried out Fourier transform infrared (FTIR) spectra to probe the coordination of FAAc on the buried interface with tin-based perovskite. As shown in **Figure 3f** and Figure S7, after introducing the SnI_2 into FAAc, the C=O stretching vibration shifted from 1720 cm^{-1} to 1710 cm^{-1}, indicating a strong coordination interaction between $Sn^{2+}$and CH_3COO^-(Ac^-).[20, 34] The C=O group donates an electron pair to coordinate with the under-coordinated Sn atoms, forming a robust C=O-Sn bond.[35] Besides, the scissoring vibration peak of N-H shifted from 1550 cm^{-1} to 1536 cm^{-1}, suggesting the formation of hydrogen bonds between Ac^- and halides.[26] The coordination between C=O and Sn^{2+}, as well as the hydrogen bonding can efficiently slow down the crystal growth rate of the subsequently deposited perovskite films, which was well consistent with the in-situ PL and in-situ UV-vis results.

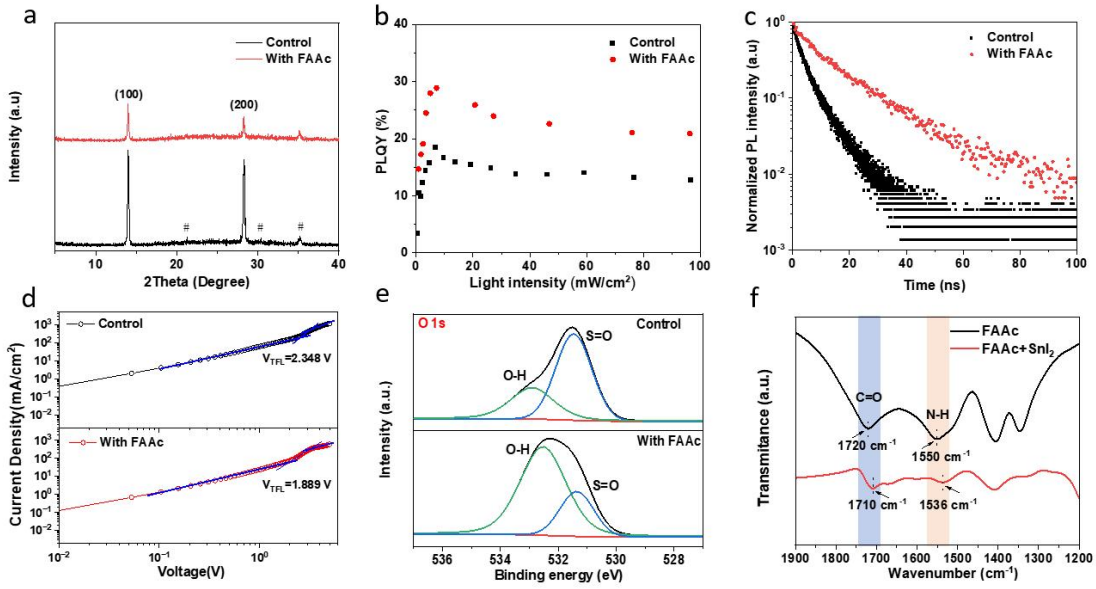

Figure 3. (a) XRD patterns, #indicates the diffraction data from the ITO substrate, (b) PLQYs, and (c) TRPL of perovskite films fabricated without and with FAAc. (d) *J-V* curves of the holy-only devices without and with FAAc modification. (e) O 1s XPS spectra of PEDOT:PSS on silicon substrate, without and with FAAc modification, and the FAAc-modified samples was washed out by DMSO. (f) FTIR spectra of FAAc and the complex of FAAc and SnI_2.

To evaluate the effect of the surface modification by FAAc molecule on devices performance, PeLEDs devices were prepared by subsequential deposition of indium tin oxide (ITO)/PEDOT:PSS/Perovskite/2,2',2'-(1,3,5-Benzinetriyl)-tris(1-phenyl-1-H-benzimidazole) (TPBi)/LiF/Al (**Figure 4a**). Figure S8 shows the cross-sectional image of the device fabricated by FAAc modification. As shown in **Figure 4b**, the energy levels of FAAc-modified PEDOT:PSS shift upwards, according to the ultra-violet photoelectron spectroscopy (UPS) results (Figure S9), which facilitates the electron blocking. The change in energy band of PEDOT:PSS could be attributed to the formation of hydrogen bonds between PSS and FAAc, thereby regulating the surface potential and energy levels of PEDOT:PSS.[36] The energy level of ITO, perovskite, TPBi and LiF/Al are taken from references.[10, 11] Different concentrations of FAAc on PEDOT:PSS substrate were investigated (Figure S10). When the PEDOT:PSS was

treated with the optimal concentration of FAAc, the peak EQE and radiance of the champion PeLEDs increased from 8.2% and 47 W sr^{-1} m^{-2} to 11.9% and 56 W sr^{-1} m^{-2} (**Figure 4c**, **d**), which is comparable to the highest reported efficiencies for near-infrared Sn-based PeLEDs (Figure S11).[11] The normalized EL peaks of two PeLEDs are 896nm and 894nm, respectively (**Figure 4e**). It is worth noting that the operational lifetime improved significantly through our BIM strategy (Figure S12a), due to the fewer defects in the perovskite films with FAAc modification. And the shapes of EL spectra for both devices remain unchanged at various voltages (Figure S12b-c). To observe the luminescence of the devices, the NIR photographs of both devices at different operating voltages were recorded by an NIR camera (Figure S13).

Additionally, the FAAc was added into perovskite solution directly. The results revealed that the morphology, PLQY and TRPL of the perovskite film were comparable to the control sample (Figure S14). Consequently, no significant enhancement in device performance was observed (Figure S15**)**. Similarly, the effect of DMSO interface treatment and FAAc post treatment (on top of perovskite) was not significant (Figure S16 and Figure S17), further indicating the effectiveness of FAAc at the buried interface. To verify which component in FAAc plays a major role in improving device performance, we compared it with the interface modifiers of MAAc and FAI. As shown in Figure S18, the devices based on MAAc exhibit significantly improved EQE compared to the PeLEDs based on FAI interface modification. These results further demonstrate that the buried interface greatly affects the performance of tin-based PeLEDs, and modifiers with carboxyl can be a general strategy for obtaining high- quality tin-based perovskite films and efficient devices. Moreover, the average peak EQEs of PeLEDs fabricated on FAAc-modified substrates is 9.6% (**Figure 4f**), suggesting that the buried-interface-modification (BIM) strategy has high reproducibility.

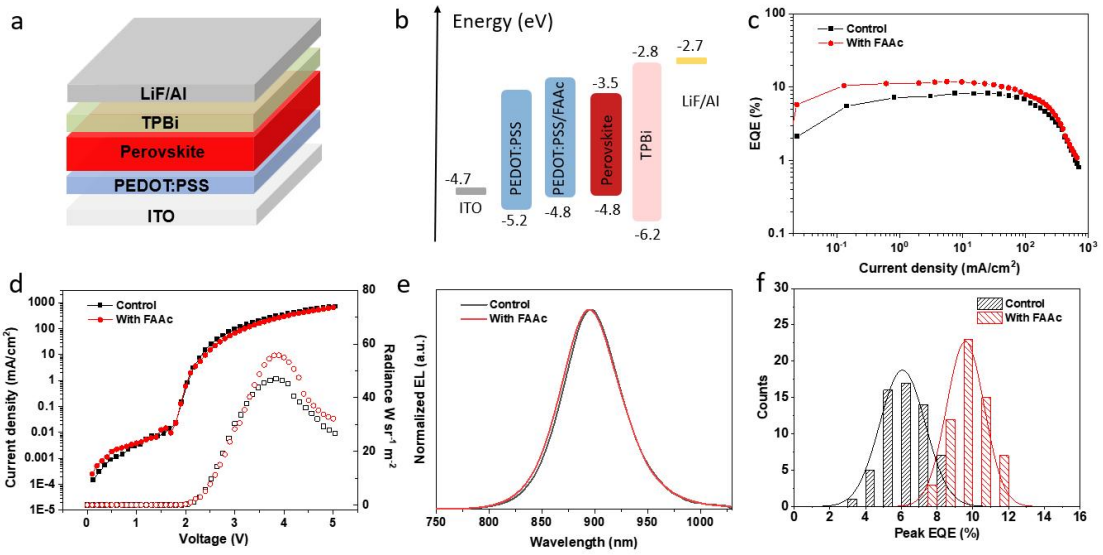

Figure 4. (a, b) Schematic illustration of the device architecture (a) and energy-level diagram (b). (c-f) EQE-*J* curve (c), *J*-*V*-*R* curve (d), EL spectra (e) and histograms of maximum EQE (f) based on $FA_{0.9}Cs_{0.1}SnI_3$ perovskite films without and with FAAc.

Conclusions

In summary, we demonstrated the critical role of buried interface on the crystallization of Sn-based perovskites. The BIM strategy can significantly regulate the nucleation sites and crystallization rate, avoiding the aggregation of perovskite grains, thereby obtaining high-quality tin-based perovskite films with smaller grains and lower defect density. We demonstrated that the carboxylate, such as FAAc and MAAc can reduce Gibbs free energy of the perovskites by forming denser hydrogen-bonding network on PEDOT:PSS substrates, thereby reducing contact angle and increasing nucleation sites. Additionally, modifiers with a strong coordination ability with Sn^{2+} are more effective to achieve high crystal quality by regulating the crystallization kinetics, leading to improved electroluminescence efficiency. As a result, the near-infrared PeLEDs based on $FA_{0.9}Cs_{0.1}SnI_3$ perovskite films on the FAAc-modified substrates exhibited a high peak EQE of 11.9% with a radiance of 56 W sr^{-1} m^{-2}. Our work provided an efficient and low-cost route for fabricating high-performance Sn-based perovskite optoelectronics.

Acknowledgements

This work was financially supported by Natural Science Foundation of Jiangsu Province, China (BK20240564), National Natural Science Foundation of China (52403327, 62475115, 22372078), National Key Research and Development Program of China (2022YFE0207600), and the Priority Academic Program Development of Jiangsu Higher Education Institutions.

Conflict of Interest

The authors declare no conflict of interest.

Data Availability Statement

The data that support the findings of this study are available from the corresponding author upon reasonable request.

References

1. G. Pacchioni, Highly efficient perovskite LEDs. *Nat. Rev. Mater.* **2021,** *6* (2), 108-108.
2. A. Fakharuddin，M. K. Gangishetty，M. Abdi-Jalebi，S.-H. Chin，A. R. bin Mohd Yusoff，D. N. Congreve，W. Tress，F. Deschler，M. Vasilopoulou，H. J. Bolink, Perovskite light-emitting diodes. *Nat. Electron.* **2022,** *5* (4), 203-216.
3. J. S. Kim，J.-M. Heo，G.-S. Park，S.-J. Woo，C. Cho，H. J. Yun，D.-H. Kim，J. Park，S.-C. Lee，S.-H. Park, Ultra-bright, efficient and stable perovskite light-emitting diodes. *Nature* **2022,** *611* (7937), 688-694.
4. Y. Sun，L. Ge，L. Dai，C. Cho，J. Ferrer Orri，K. Ji，S. J. Zelewski，Y. Liu，A. J. Mirabelli，Y. Zhang, Bright and stable perovskite light-emitting diodes in the near-infrared range. *Nature* **2023,** *615* (7954), 830-835.
5. M. Li，Y. Yang，Z. Kuang，C. Hao，S. Wang，F. Lu，Z. Liu，J. Liu，L. Zeng，Y. Cai, Acceleration of radiative recombination for efficient perovskite LEDs. *Nature* **2024**, 1-5.
6. S. C. Feng，Y. Shen，X. M. Hu，Z. H. Su，K. Zhang，B. F. Wang，L. X. Cao，F. M. Xie，H. Z. Li，X. Gao, Efficient and stable red perovskite light-emitting diodes via thermodynamic crystallization control. *Adv. Mater.* **2024**, 2410255.
7. Z. Xing，G. Jin，Q. Du，P. Pang，T. Liu，Y. Shen，D. Zhang，B. Yu，Y. Liang，D. Yang, Ions

‐induced assembly of perovskite nanocomposites for highly efficient light-emitting diodes with EQE exceeding 30%. *Adv. Mater.* **2024**, 2406706.

8. W. Ke，M. G. Kanatzidis, Prospects for low-toxicity lead-free perovskite solar cells. *Nat. Commun.* **2019,** *10* (1), 965.

9. H. Zhang，J.-W. Lee，G. Nasti，R. Handy，A. Abate，M. Grätzel，N.-G. Park, Lead immobilization for environmentally sustainable perovskite solar cells. *Nature* **2023,** *617* (7962), 687-695.

10. H. Min，J. Chang，Y. Tong，J. Wang，F. Zhang，Z. Feng，X. Bi，N. Chen，Z. Kuang，S. Wang, Additive treatment yields high-performance lead-free perovskite light-emitting diodes. *Nat. Photonics* **2023,** *17* (9), 755-760.

11. H. Min，N. Wang，N. Chen，Y. Tong，Y. Wang，J. Wang，J. Liu，S. Wang，X. Wu，P. Yang, Spin coating epitaxial heterodimensional tin perovskites for light-emitting diodes. *Nat. Nanotechnol.* **2024,** *19* (5), 632-637.

12. F. Yuan，G. Folpini，T. Liu，U. Singh，A. Treglia，J. W. M. Lim，J. Klarbring，S. I. Simak，I. A. Abrikosov，T. C. Sum, Bright and stable near-infrared lead-free perovskite light-emitting diodes. *Nat. Photonics* **2024,** *18* (2), 170-176.

13. X. Guan，Y. Li，Y. Meng，K. Wang，K. Lin，Y. Luo，J. Wang，Z. Duan，H. Liu，L. Yang, Targeted elimination of tetravalent-Sn-induced defects for enhanced efficiency and stability in lead-free NIR-II perovskite LEDs. *Nat. Commun.* **2024,** *15* (1), 9913.

14. F. Zhang，H. Min，Y. Zhang，Z. Kuang，J. Wang，Z. Feng，K. Wen，L. Xu，C. Yang，H. Shi, Vapor-assisted in situ recrystallization for efficient tin-based perovskite light-emitting diodes. *Adv. Mater.* **2022,** *34* (37), 2203180.

15. T. Li，Z. Zhang，F. He，L. Deng，Y. Yang，X. Mo，Y. Zhan，J. Liang, Alleviating the crystallization dynamics and suppressing the oxidation process for tin-based perovskite solar cells with fill factors exceeding 80 percent. *Adv. Funct.Mater.* **2023,** *33* (51), 2308457.

16. M. Yin，H. Yao，H. Qiu，C. Wu，M. Zhang，F. Hao, A Revisit of Crystallization in Tin Halide Perovskite Thin Films: From Nucleation, Intermediate to Crystal Growth. *Adv. Funct.Mater.* **2024,** *34* (39), 2404792.

17. Y. Zhang，C. Li，H. Zhao，Z. Yu，X. Tang，J. Zhang，Z. Chen，J. Zeng，P. Zhang，L. Han, Synchronized crystallization in tin-lead perovskite solar cells. *Nat. Commun.* **2024,** *15* (1), 6887.

18. S. Liu，J. Li，W. Xiao，R. Chen，Z. Sun，Y. Zhang，X. Lei，S. Hu，M. Kober-Czerny，J. Wang, Buried interface molecular hybrid for inverted perovskite solar cells. *Nature* **2024,** *632* (8025), 536-542.

19. C. Luo，G. Zheng，F. Gao，X. Wang，C. Zhan，X. Gao，Q. Zhao, Engineering the buried interface in perovskite solar cells via lattice-matched electron transport layer. *Nat. Photonics* **2023,** *17* (10), 856-864.

20. Y. Liu，T. Niu，J. Wang，Y. Li，N. Meng，B. Yu，X. Shi，K. Xu，J. Chen，D. Ma，Y. Xia，Q. Guo，Y. Chen, Regulating the grain-growth surface for efficient near-infrared perovskite light-emitting diodes. *Nano Lett.* **2024,** *24* (35), 10972-10979.

21. G. Chen，S. Wang，Z. Yu，C. Dong，P. Jia，D. Pu，K. Dong，H. Cui，H. Fang，C. Wang, Regulation of nucleation and crystallization for blade-coating large-area $CsPbBr_3$ perovskite light-emitting diodes. *Sci. Bull.* **2024,** *70* (2), 210-222.

22. J. Jiang，M. Shi，Z. Xia，Y. Cheng，Z. Chu，W. Zhang，J. Li，Z. Yin，J. You，X. Zhang, Efficient pure-red perovskite light-emitting diodes with strong passivation via ultrasmall-sized molecules. *Sci. Adv.* **2024,** *10* (18), eadn5683.

23. X. Sun，H. Wu，Z. Li，R. Zhu，G. Li，Z. Su，J. Zhang，X. Gao，J. Pascual，A. Abate, Multifunctional modification of the buried interface in mixed tin-lead perovskite solar cells. *Angew. Chem., Int. Ed.* **2024,** *63* (48), e202409330.

24. X. Ling，H. Zhu，W. Xu，C. Liu，L. Pan，D. Ren，J. Yuan，B. W. Larson，C. Grätzel，A. R. Kirmani, Combined precursor engineering and grain anchoring leading to MA-free, phase-pure, and stable α-formamidinium lead iodide perovskites for efficient solar cells. *Angew. Chem., Int. Ed.* **2021,** *60* (52), 27299-27306.

25. L. Duan，H. Zhang，M. Liu，M. Grätzel，J. Luo, Phase-pure γ-$CsPbI_3$ for efficient inorganic perovskite solar cells. *ACS Energy Lett.* **2022,** *7* (9), 2911-2918.

26. S. Wang，H. Yao，W. Zhu，C. Wu，Z. Tang，J. Liu，L. Ding，F. Hao, Stabilization of perovskite lattice and suppression of Sn^{2+}/Sn^{4+} oxidation via formamidine acetate for high efficiency tin perovskite solar cells. *Adv. Funct. Mater.* **2023,** *33* (17), 2215041.

27. T. Niu，L. Chao，Y. Xia，K. Wang，X. Ran，X. Huang，C. Chen，J. Wang，D. Li，Z. Su, Phase-pure α-$FAPbI_3$ perovskite solar cells via activating lead-iodine frameworks. *Adv. Mater.* **2024,** *36* (13), 2309171.

28. A. Liu，Z. Zhang，J. Li，H. Yu，N. Wang，J. Wang，N. Zhao, Optimizing perovskite surfaces to enhance post-treatment for efficient blue mixed-halide perovskite light-emitting diodes. *Adv. Mater.* **2024**, 2414788.

29. X. Zhu，Z. Xu，T. Zhang，J. Zhang，Y. Guo，M. Shan，K. Wang，T. Shi，G. Cui，F. Wang, Ultra-stable zinc anodes facilitated by hydrophilic polypropylene separators with large scale production capacity. *Adv. Funct. Mater.* **2024,** *34* (44), 2407262.

30. M. Jung，S.-G. Ji，G. Kim，S. I. Seok, Perovskite precursor solution chemistry: from fundamentals to photovoltaic applications. *Chem. Soc. Rev.* **2019,** *48* (7), 2011-2038.

31. Y. Deng，C. H. Van Brackle，X. Dai，J. Zhao，B. Chen，J. Huang, Tailoring solvent coordination for high-speed, room-temperature blading of perovskite photovoltaic films. *Sci. Adv.* **2019,** *5* (12), eaax7537.

32. X. Luo，W. Xu，G. Zheng，S. Tammireddy，Q. Wei，M. Karlsson，Z. Zhang，K. Ji，S. Kahmann，C. Yin, Effects of local compositional heterogeneity in mixed halide perovskites on blue electroluminescence. *Matter* **2024,** *7* (3), 1054-1070.

33. M. A. Lampert, Simplified theory of space-charge-limited currents in an insulator with traps. *Phys. Rev.* **1956,** *103* (6), 1648.

34. W. Pan，J. Lin，J. Wu，B. Rong，X. Zhang，Q. Chen，M. Zhang，S. Wang，W. Sun，X. Wang, Interface modification by formamidine acetate for efficient perovskite solar cells. *Solar Energy* **2022,** *232*, 304-311.

35. Y. Sun，R. Hu，F. Wang，T. Wang，X. Liang，X. Zhou，G. Yang，Y. Li，F. Zhang，Q. Zhu, Ionic liquid-regulated PbI_2 layers and defect passivation for efficient perovskite solar cells. *J. Mater. Chem. C* **2024,** *12* (14), 5175-5183.

36. T. Li，J. Xu，R. Lin，S. Teale，H. Li，Z. Liu，C. Duan，Q. Zhao，K. Xiao，P. Wu, Inorganic wide-bandgap perovskite subcells with dipole bridge for all-perovskite tandems. *Nat. Energy* **2023,** *8* (6), 610-620.

Supplementary Information

A Buried-Interface-Modification Strategy for Efficient Tin-Based Perovskite Light-Emitting Diodes

Zheng Jiang[1#], Jie Yang,[2#] Wenbin Wang[1], Yangyu Liu[3], Yuhan Zhou[3], Jing Xu[3], Wang Wang[2], Hongyao Ding[1], Ya Zhong[1], Haifeng Zhao[4,5], Sai Bai[4], Weidong Xu[6], Wing Chung Tsoi[8], Tao Yu[3], Chunxiong Bao[3], Xiaodong Shen[1]*, Pengpeng Teng [1,7]*

[1]Jiangsu Collaborative Innovation Center for Advanced Inorganic Functional Composites, College of Materials Science and Engineering, Nanjing Tech University, Nanjing, 211816 China

[2]Key Laboratory of Flexible Electronics (KLOFE), Institute of Advanced Materials (IAM) & School of Flexible Electronics (Future Technologies), Nanjing Tech University (NanjingTech), Nanjing, China

[3]National Laboratory of Solid State Microstructures, Collaborative Innovation Center of Advanced Microstructures, School of Physics, Nanjing University, Nanjing 210093, China

[4]Institute of Fundamental and Frontier Science, University of Electronic Science and Technology of China (UESTC), Chengdu 610054, China

[5]Yibin Institute of UESTC, University of Electronic Science and Technology of China (UESTC), Yibin 644005，China

[6]Institute of Flexible Electronics (IFE), Northwestern Polytechnical University, 127 West Youyi Road, Xi'an 710072, China.

[7]Quechen Silicon Chemical Co., Ltd

[8]SPECIFIC, Faculty of Science and Engineering, Swansea University, Bay Campus, Fabian Way, Swansea SA1 8EN, United Kingdom.

[#] These authors contributed equally: Zheng Jiang and Jie Yang.

*Correspondence to Xiaodong Shen (xdshen@njtech.edu.cn); Pengpeng Teng (ppteng@njtech.edu.cn).

Experimental Section

Synthesis and materials preparation

The molar ratio of FAI, CsI, SnI_2, PEAI, SnF_2 and VmB1in the perovskite solution is 0.9: 0.1: 1.0: 0.2: 0.2: x. For the preparation of 1 mL of perovskite solution, a 500 mg/ml FAI solution, a 100 mg/ml PEAI solution, and a 100 mg/ml CsI solution were first prepared using DMSO as the solvent. VmB1, SnI_2, and SnF_2 were then dissolved in a mixed solvent of DMF/DMSO (v/v = 1:4, 14 wt%) with a molar ratio of x: 1: 0.2. Additionally, 0.02 M Sn powder was added to suppress the oxidation of Sn^{2+}. The FAI solution, PEAI solution, and CsI solution were dripped into the precursor solution according to the molar ratio of FAI: CsI: SnI_2: PEAI = 0.9: 0.1: 1: 0.2. After thorough mixing, the solution was filtered. PEDOT:PSS (Clevios P VP4083) was diluted in deionized water with a v/v ratio of 1:4. The modifying material was dissolved in DMSO to obtain solutions of FAAc, MAAc and FAI. TPBi (Xi'an Polymer Light Technology Corp, 99.9%) and LiF (Shanghai Han Feng Chemical Co., Ltd, 99.9%) were used as received.

Device fabrication

The LED devices were fabricated on ITO-coated glass substrates with an area of 2.5 mm^2. The PEDOT:PSS was deposited on the ITO glass as hole transport layer at a speed of 5,000 rpm for 50 s and then annealed at 150°C for 10 min. Next, the FAAc solution was spin-coated on the PEDOT:PSS film at a speed of 4,000 rpm for 30 s, followed by annealing at 100°C for 10 min. Subsequently, the perovskite layer was prepared by spin-coating the perovskite precursor solution onto the modifying layer FAAc film at a speed of 5,500 rpm for 60 s, and then annealed at 65°C for 5 min. Finally, the TPBi, LiF, and Al layers were thermally evaporated. The holy-only devices were fabricated with the structure of ITO/PEDOT:PSS/Perovskite/PTAA/Al.

Characterizations

The device was characterized inside a nitrogen-filled glovebox via a system

comprising a Keithley 2440 5A SourceMeter, a fiber-optic integrating sphere (FOIS-1), and a NOVA2S spectrometer. All measurements were carried out without imposing any bias voltage on the devices. The ultraviolet-visible (UV-vis) absorption spectrum was obtained by employing a spectrophotometer equipped with an integrating sphere. The photoluminescence spectre were recorded with a NOVA2S spectrometer, utilizing a 375 nm continuous wave (CW) laser as the excitation source. In-situ photoluminescence (PL) spectra were also collected by using a NOVA2S spectrometer and excited with a 375 nm CW laser. The photoluminescence quantum efficiency (PLQE) was determined by means of an integrating sphere system and a 375 nm CW laser acting as the excitation source. Time-resolved PL measurements were performed with an Edinburgh Instruments Spectrometer (FLS980) with a 375 nm pulsed laser for excitation. X-ray diffraction (XRD) data were collected using a Rigaku D/MAX-Ultima III diffractometer. Scanning electron microscopy (SEM) images were obtained with a Zeiss G500 high-resolution SEM. The Fourier transform Infrared spectra (FTIR) measurement were characterized by PE-Spectrum Two in transmittance model. Ultraviolet photoelectron spectroscopy (UPS) measurements were carried out using an AXIS SUPRA+ instrument. X-ray photoelectron spectroscopy (XPS) spectra were acquired with an AXIS SUPRA+ X-ray photoelectron spectrometer. To avoid atmospheric exposure, all samples were transferred to the XPS chamber through a nitrogen-filled glovebox to avoid atmospheric exposure. The samples for STEM and HAADF images were prepared using an FEI Helios dual-beam FIB workstation equipped with an in-situ micromanipulator and Pt gas injection system.

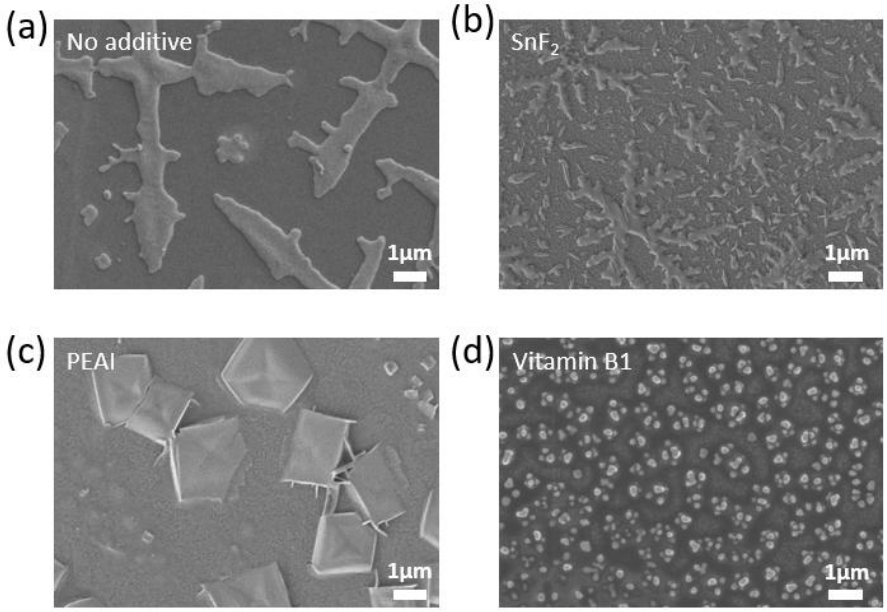

Figure S1. SEM images of $FA_{0.9}Cs_{0.1}SnI_3$ perovskite films with different additives. (a) No additive, (b) SnF_2, (c) PEAI and (d) Vitamin B1

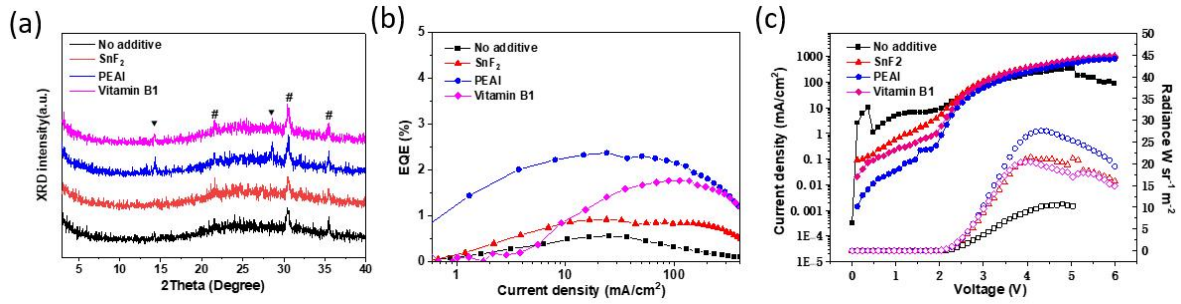

Figure S2. (a) XRD patterns of perovskite films with different additives, #indicates the diffraction data from the ITO substrate, (b) EQE-*J* curve and (c) *J*-*V*-*R* curve of tin-based PeLEDs based on different additives.

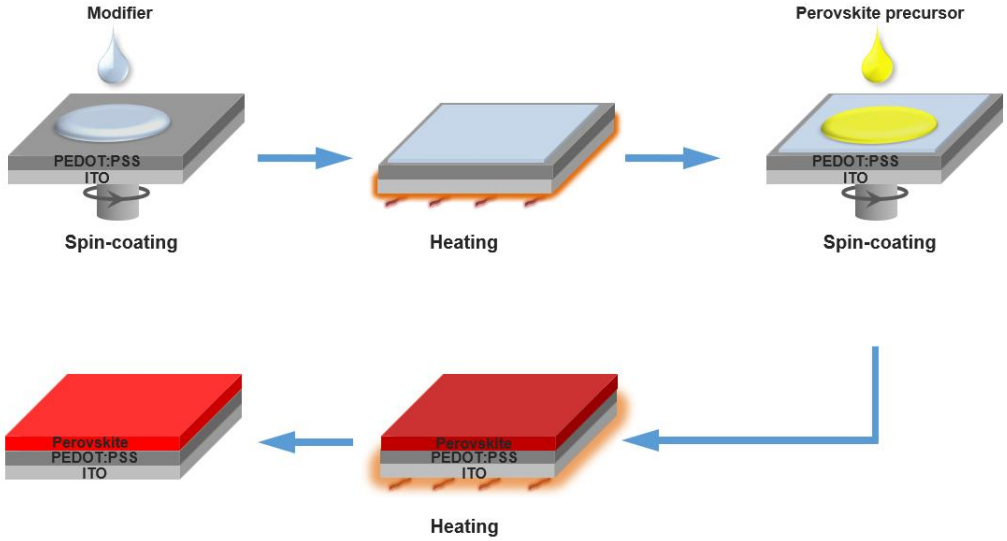

Figure S3. Schematic process for preparation of Sn-based perovskite films through buried-interface modification with modifier.

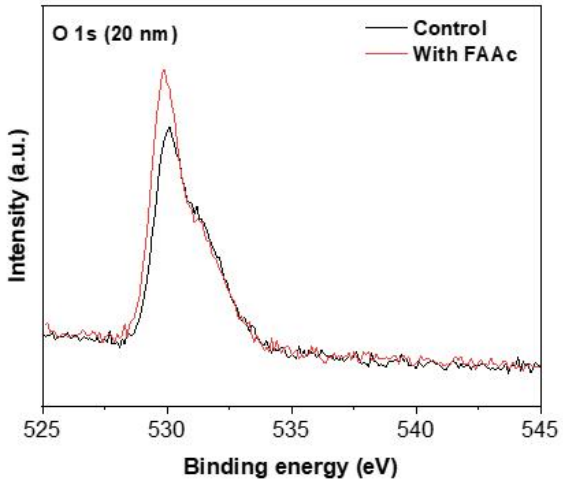

Figure S4. XPS core level spectra of O 1s for the tin-based provskite films without and with FAAc on silicon substrates under the depth of 20 nm.

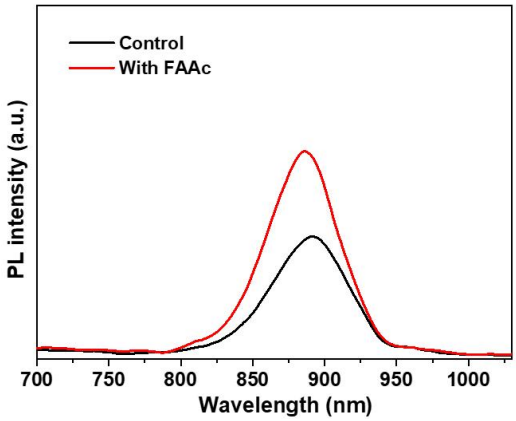

Figure S5. PL spectra of Sn-based perovskite films without and with FAAc modification at room temperature.

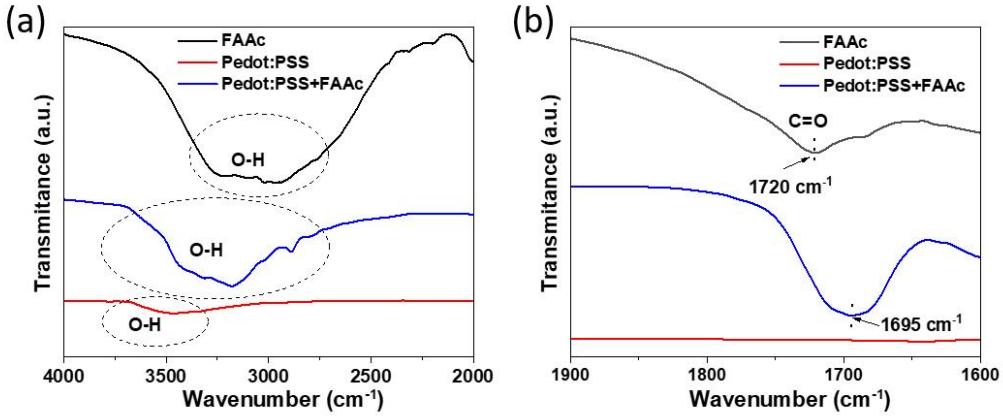

Figure S6. FTIR spectra of PEDOT:PSS, FAAc and the complex of PEDOT:PSS and FAAc.

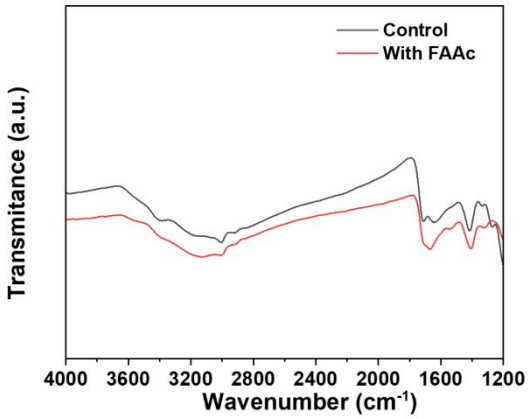

Figure S7. FTIR spectra of Sn-based perovskite films without and with FAAc.

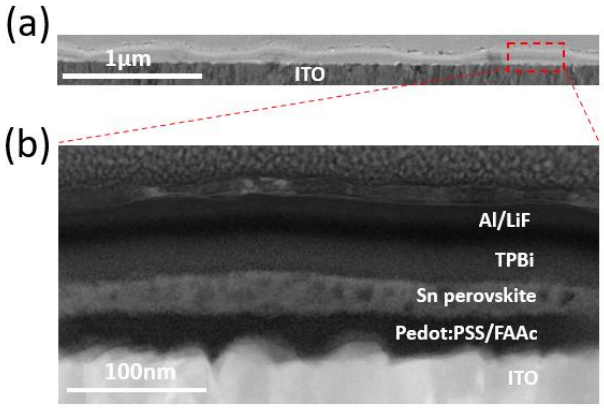

Figure S8. (a) STEM and (b) HAADF images of the tin-based perovskite device.

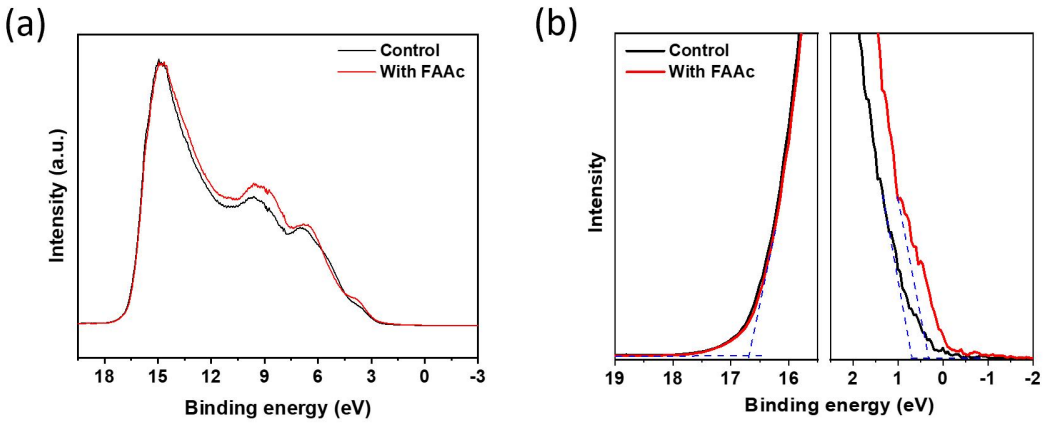

Figure S9. UPS spectra (He I= 21.22 eV) of PEDOT:PSS without and with FAAc modification on silicon substrate. The FAAc samples were washed out by DMSO.

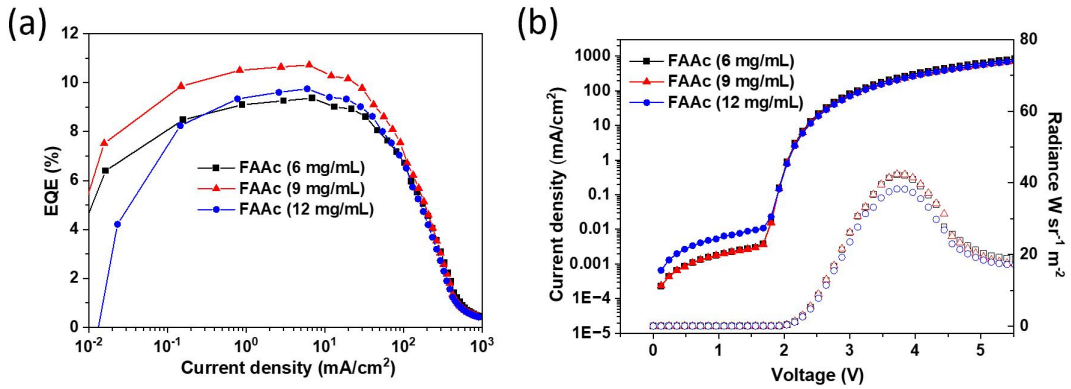

Figure S10. The EQE-*J* curve (a) and *J*-*V*-*R* curve (b) of tin-based PeLEDs with different concentrations of FAAc.

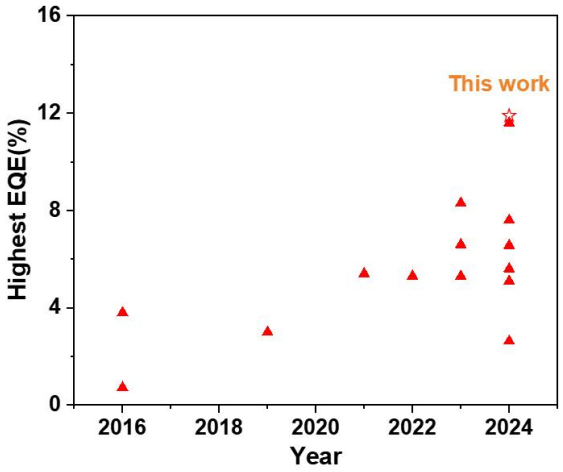

Figure S11. Development of near-infrared Sn-based PeLEDs.[1-15]

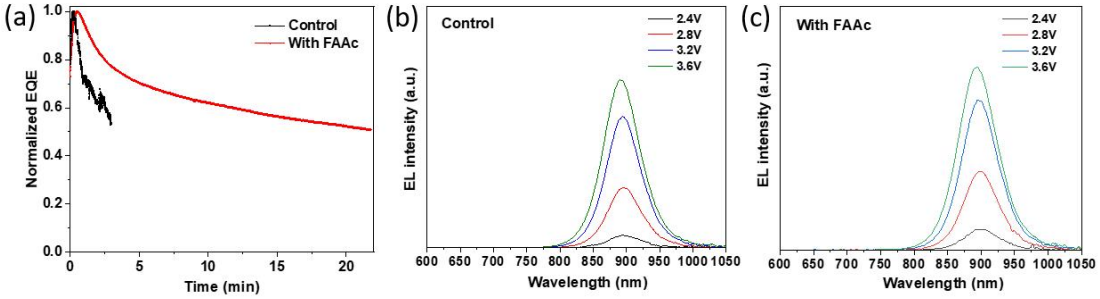

Figure S12. (a) Operational stability of Sn-based perovskite devices without and with FAAc at a constant density of 1 mA/cm^2. EL spectra of devices without (b) and with FAAc (c) under various voltages.

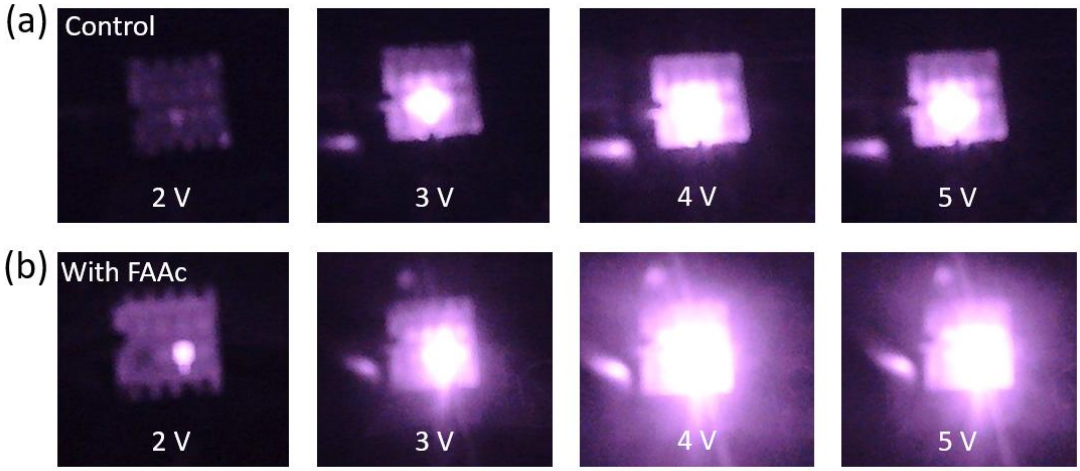

Figure S13. NIR photographs of tin-based perovskite devices without and with FAAc at different bias

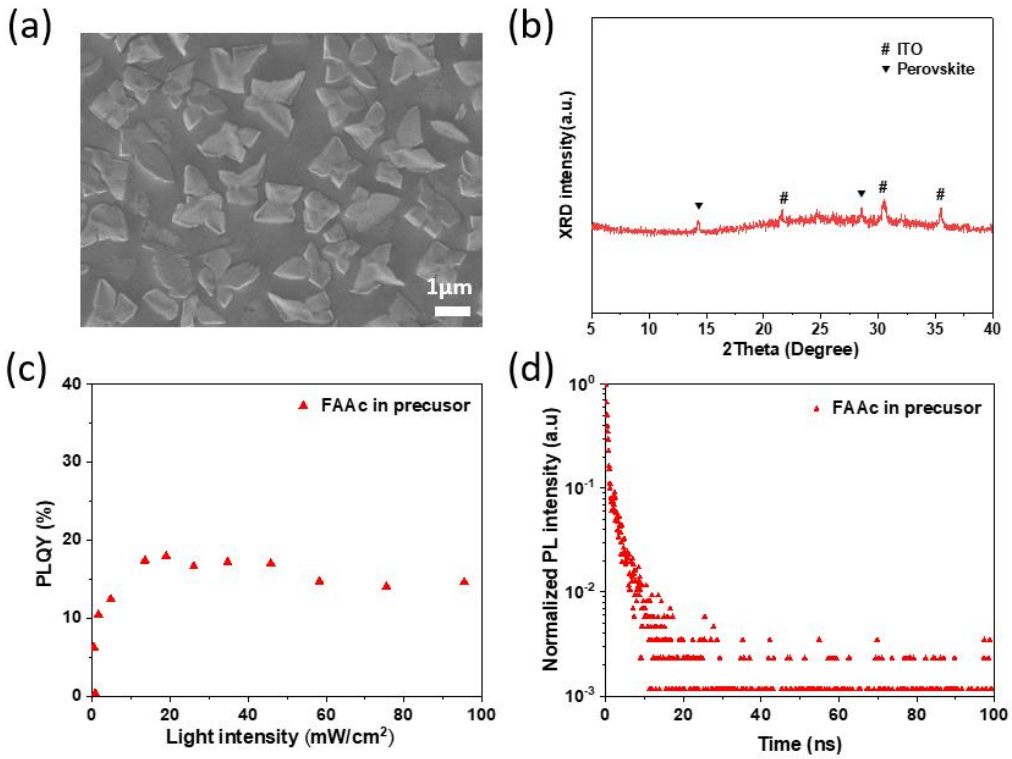

Figure S14. (a) SEM image, (b) XRD pattern, (c) PLQY, and (d) TRPL of tin-based perovskite film with FAAc in perovskite solution.

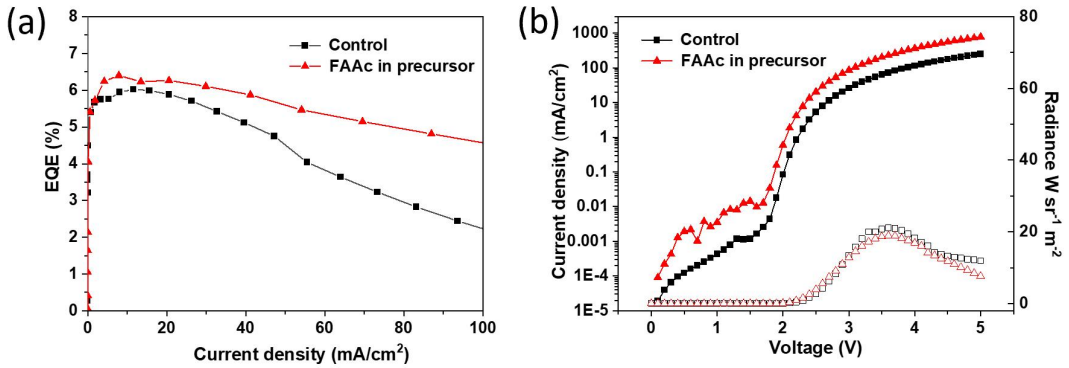

Figure S15. The EQE-*J* curve (a) and *J*-*V*-*R* curve (b) of tin-based PeLEDs with and without FAAc in perovskite solution. The content of FAAc in precursor was optimized.

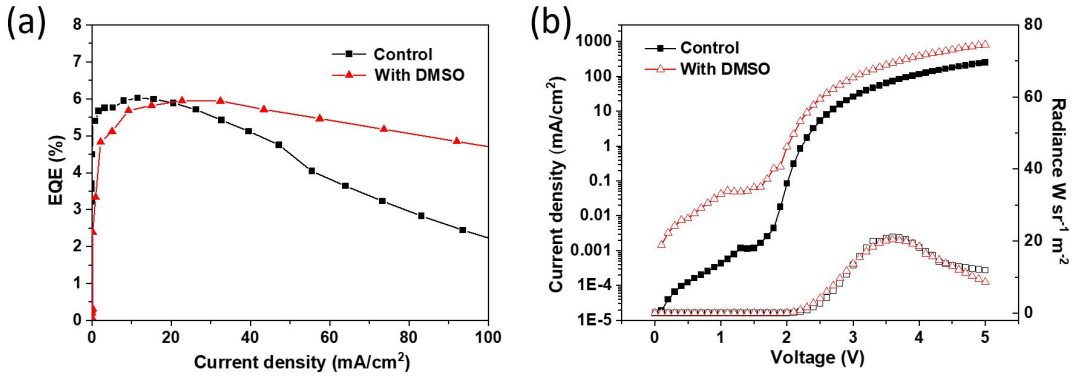

Figure S16. The EQE-*J* curve (a) and *J-V-R* curve (b) of tin-based PeLEDs with and without DMSO treatment.

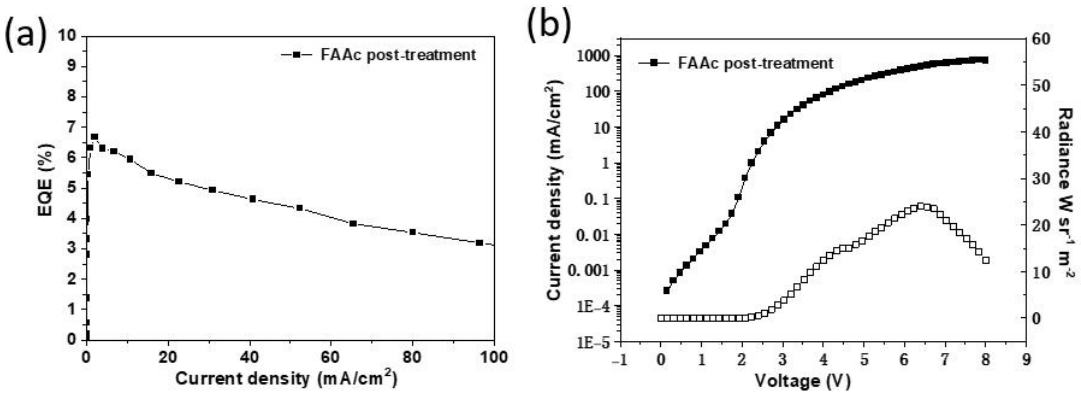

Figure S17. The EQE-J curve (a) and J-V-R curve (b) of tin-based PeLEDs post treated by FAAc.

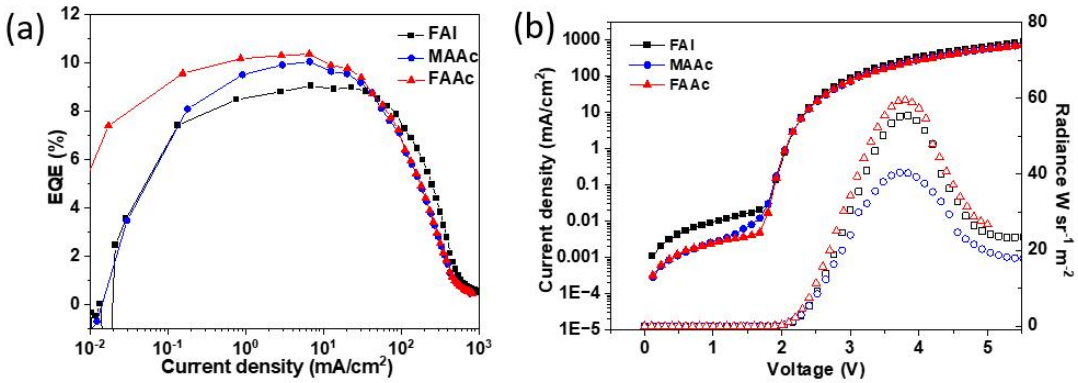

Figure S18. The EQE-*J* curve (a) and *J-V-R* curve (b) of tin-based PeLEDs modified by FAI, MAAc and FAAc.

Supplementary Table 1. A summary of PeLED characteristics with different additives.

Additives	EL(nm)	FWHM(nm)	R (W sr^{-1} m^{-2})	EQE(%)
None	896	62	5±4(15)	0.2±0.1(0.3)
SnF_2	896	61	15±9(20)	0.5±0.1(0.6)
PEAI	896	70	19±9(25)	2.0±0.4(2.5)
Vitamin B1	892	63	14±9(20)	1.5±0.3(2.0)
Control	896	69	38±13(45)	7.5±0.8(8.4)

Summarized from ten individual devices.

References

1. M. L. Lai, T. Y. Tay, A. Sadhanala, S. E. Dutton, G. Li, R. H. Friend, Z.-K. Tan, Tunable near-infrared luminescence in tin halide perovskite devices. *J. Phys. Chem. Lett.* **2016,** *7* (14), 2653-2658.
2. W.-L. Hong, Y.-C. Huang, C.-Y. Chang, Z.-C. Zhang, H.-R. Tsai, N.-Y. Chang, Y.-C. Chao, Efficient low-temperature solution-processed lead-free perovskite infrared light-emitting diodes. *Adv. Mater.* **2016,** *28* (36), 8029-8036.
3. Y. Wang, R. Zou, J. Chang, Z. Fu, Y. Cao, L. Zhang, Y. Wei, D. Kong, W. Zou, K. Wen, Tin-based multiple quantum well perovskites for light-emitting diodes with improved stability. *J. Phys. Chem. Lett.* **2019,** *10* (3), 453-459.
4. J. Wang, J. Dong, F. Lu, C. Sun, Q. Zhang, N. Wang, Two-dimensional lead-free halide perovskite materials and devices. *J. Mater. Chem. A.* **2019,** *7* (41), 23563-23576.
5. J. Lu, X. Guan, Y. Li, K. Lin, W. Feng, Y. Zhao, C. Yan, M. Li, Y. Shen, X. Qin, Dendritic $CsSnI_3$ for efficient and flexible near-infrared perovskite light-emitting diodes. *Adv. Mater.* **2021,** *33* (44), 2104414.
6. F. Zhang, H. Min, Y. Zhang, Z. Kuang, J. Wang, Z. Feng, K. Wen, L. Xu, C. Yang, H. Shi, Vapor-assisted in situ recrystallization for efficient tin‐based perovskite light-emitting diodes. *Adv. Mater.* **2022,** *34* (37), 2203180.
7. X. Guan, J. Lu, Q. Wei, Y. Li, Y. Meng, K. Lin, Y. Zhao, W. Feng, K. Liu, G. Xing, Suppressing disproportionation decomposition in Sn-based perovskite light-emitting diodes. *ACS Energy Lett.* **2023,** *8* (3), 1597-1605.
8. G. Zhang, S. Xing, X. Cao, B. Zhao, D. Di, Stabilizing FASnI 3-based perovskite light-emitting diodes with crystallization control. *Nanoscale* **2023,** *15* (15), 6954-6959.
9. H. Min, J. Chang, Y. Tong, J. Wang, F. Zhang, Z. Feng, X. Bi, N. Chen, Z. Kuang, S. Wang, Additive treatment yields high-performance lead-free perovskite light-emitting diodes. *Nat. Photonics* **2023,** *17* (9), 755-760.
10. Y. Li, X. Guan, Y. Meng, J. Chen, J. Lin, X. Chen, C. Y. Liu, Y. Zhao, Q. Zhang, C. Tian, Boosting $CsSnI_3$-based near-infrared perovskite light-emitting diodes performance via solvent

coordination engineering. *InfoMat* **2024,** *6* (5), e12537.
11. H. Min, N. Wang, N. Chen, Y. Tong, Y. Wang, J. Wang, J. Liu, S. Wang, X. Wu, P. Yang, Spin coating epitaxial heterodimensional tin perovskites for light-emitting diodes. *Nature Nanotechnology* **2024,** *19* (5), 632-637.
12. F. Yuan, G. Folpini, T. Liu, U. Singh, A. Treglia, J. W. M. Lim, J. Klarbring, S. I. Simak, I. A. Abrikosov, T. C. Sum, Bright and stable near-infrared lead-free perovskite light-emitting diodes. *Nat. Photonics* **2024,** *18* (2), 170-176.
13. Y. Shen, Z. Tang, J. Chen, T. Zhang, L. Qian, C. Xiang, The improvement of tin-based perovskite thin film quality to enhance the performance of near-infrared peleds through thiocyanate modification. *Adv. Opt. Mater.* **2024,** *12* (20), 2400398.
14. Q. Teng, J. Li, J. Li, X. Yan, C. Li, Q. Tan, W. Qin, J. He, F. Yuan, Localized electron density engineering for bright and stable near-infrared electroluminescence from all-inorganic lead-free tin halides. *ACS Energy Lett.* **2024,** *9* (10), 4785-4791.
15. X. Guan, Y. Li, Y. Meng, K. Wang, K. Lin, Y. Luo, J. Wang, Z. Duan, H. Liu, L. Yang, Targeted elimination of tetravalent-Sn-induced defects for enhanced efficiency and stability in lead-free NIR-II perovskite LEDs. *Nat. Commun.* **2024,** *15* (1), 9913.